RSC Advances

Facile synthesis of water soluble silver ferrite (AgFeO2) nanoparticles and their biological application as antibacterial agents

SCHOLARONE™
Manuscripts

Facile synthesis of water soluble silver ferrite (AgFeO$_2$) nanoparticles and their biological application as antibacterial agents

Hani Nasser Abdelhamid [1,2], Abuo Talib,[5] Hui-Fen Wu[1,3,4,5,6]*

[1]Department of Chemistry, National Sun Yat-Sen University, Kaohsiung, 804, Taiwan
[2]Department of Chemistry, Assuit University, Assuit, 71515, Egypt
[3]School of Pharmacy, College of Pharmacy, Kaohsiung Medical University, Kaohsiung, 800, Taiwan
[4]Center for Nanoscience and Nanotechnology, National Sun Yat-Sen University, Kaohsiung, 804, Taiwan
[5]Doctoral Degree Program in Marine Biotechnology, National Sun Yat-Sen University, Kaohsiung, 804, Taiwan
[6]Medical Science and Technology, National Sun Yat-Sen University, Kaohsiung, 804, Taiwan
*Corresponding author. Tel: 886-7-5252000-3955. Fax: 886-7-525-3908.
E-mail: hwu@faculty.nsysu.edu.tw (Prof. Hui-Fen Wu)

Abstract

The synthesis as well as the antibacterial activity of AgFeO$_2$ and AgFO$_2$ modified polyethylene glycol (PEG) was reported. The antibacterial activity was investigated against different pathogenic bacteria for water treatment. The antibacterial activities were quantified by counted the colonies formed in a petri dish, a method called plate counting, and by measuring the turbidity using optical density at wavelength 600 nm (OD$_{600}$). AgFeO$_2$ NPs offer high antibacterial efficiency and can be easily separated from the solution using small external magnetic bar. The data revealed that higher concentration led to high potency. PEG was not only mitigates the cytotoxicity of AgFeO$_2$, protects magnetic core, but also improves the dispersion of the AgFeO$_2$ NPs. Because of their superior cytotoxicity and magnetic property, this antibacterial material may has great potential in biomedical applications in the near future.

Keywords: silver, magnetic nanoparticles, pathogenic bacteria, antibacterial, cell proteomic

Introduction

Pathogenic microorganisms such as bacteria in drinking water can cause many diseases, which endanger human health and become a serious problem in public healthcare [1]. Thus, it causes a serious problem. For instance, these pathogens are linked to an estimated 23,000 deaths and 2 million infections in the U.S. each year. It causes also a huge burden on the UK's health system where they consider the largest public funder of biomedical research [1]. Thus many treatment methodology and different materials were investigated for fighting those pathogens. Inorganic antibacterial materials, especially nanoparticles (NPs), have been highlighted owing to their advantages over traditionally used organic reagents in terms of long term efficacy, high chemical stability, thermal stability, flexible to further modification, and inexpensive[2]. Among various NPs, Ag has the highly antibacterial activity and has been widely used as a bactericide in over than 250+ products including dietary supplements, body soap, cloths, toys, sports products …etc (http://www.epa.gov/heasd/research/nanosilver.html) [3]. It has high antibacterial activities and easy to be modified with various inorganic [4] and organic carriers [5],. These combinations circumvent two primary drawbacks for the use of Ag NPs in water systems, which includes their aggregation and release into the environment [6]. Thus, it is combined with magnetic nanoparticles to minimize the possibility of aggregation and to improve the separation efficiency directly from the sample solutions. The main advantage of the combination between the antibacterial activity i.e use Ag and the magnetic property, use magnetic nanoparticles, is their application for water treatment. High levels of pathogenic bacteria can be indicative of poor water quality. However, magnetic NPs is easy to aggregate because of interparticle dipolar forces [7].

The most attractive combination of Ag nanoparticles is their conjugation with magnetic nanoparticles. These combinations led to add more functions such as recycling of antimicrobial materials which can be reused for many times. Among a wide range of magnetic materials, M type ferrites with the general formula of MFe_2O_4 (M = Mn, Co, Ni, Cu, or Zn) or $MFeO_2$ (Ag) are most attractive because of their magnetic and electrical properties as well as their chemical and thermal stabilities[8]. Magnetic hybrid colloids decorated with Ag nanoparticles is also investigated intensively nowadays[9]. They possess many possible forms such as $CoFe_2O_4$@polyaniline(PANI)@Ag[10], porous Fe_3O_4 shell/silver core nano composites[11], $NiFe_2O_4$@PANI@Ag[12], Fe_3O_4@Ag–PEG hybrid[13], Ag-coated Fe_3O_4@SiO_2 magnetic[14], Ag–$CuFe_2O_4$[15], Ag@Fe_3O_4–SiO_2 JNRs[16], silver coated E-33/iron oxide[17], magnetic Ni/Ag core–shell nanostructure[18], silver-coated MnZn ferrite (MZF@Ag)[19], Fe_3O_4@C@Ag[20], and magnetic graphite carbon spheres (MGCSs)@Ag[21]. The main advantage of the magnetic properties is their ability to be easily separated from aqueous solution[22]. However, Ag can be easily leached from the surface of magnetic nanoparticles.

Herein, we synthesized two forms of silver ferrite (bare and modified with polyethylene glycol, PEG) and characterize by UV-vis absorption, transmission electron microscopy (TEM), scanning electron microscopy (SEM), Fourier transform infrared (FTIR), and energy dispersive X-ray (EDX). The antibacterial of those materials were evaluated by optical density at wavelength 600 nm (OD_{600}) and plate counting method. The proteomic analysis of the cell protein corona was reported by matrix assisted laser desorption/ionization mass spectrometry (MALDI-MS). The cell morphology changes due to $AgFeO_2$ were investigated using TEM. The data revealed high antibacterial efficiency of the synthesized materials. Surface capping of $AgFeO_2$ with polyethylene glycol (PEG) mitigate the activity of material as antibacterial agents.

Materials and Methods

$Fe_2(SO_4)_3$, $AgNO_3$, polyethylene glycol (PEG), sinapic acid were purchased from Sigma-Aldrich (USA). All the chemicals used in this study are of analytical reagent grade.

Experimental

Synthesis of $AgFeO_2$

The method of $AgFeO_2$ synthesis is based on co-precipitation/hydrothermal of $Fe_2(SO_4)_3$ and $AgNO_3$ in presence of glycerol. Typically, 1 mmol of $Fe_2(SO_4)_3$ and 1 mmol $AgNO_3$ were mixed together in 30 mL of deionized water with 3 mL glycerol. Then, 10% of NaOH was added with stirring about 1h. The precipitate was transferred to Teflon autoclave and was heated at 180 ºC for 24h. The precipitate was then cooled and separated using magnet and washed several time by deionized water as shown in Scheme 1.

Preparation of $AgFeO_2$ modified polyethylene glycol ($AgFeO_2@PEG$)

About 0.5 g of the dried $AgFeO_2$ was stirred in 25 mL of aqueous PEG (2 mL). The solution was kept for stirring for 5h. The prepared material was separated using external magnet and washed using deionized water with the help of an external magnet.

Instrumentation

Scanning electron microscope (SEM, JOEL 6700F, Japan) with energy dispersive spectrometer (EDS) working at 30 kV was used to examine the surface morphology and elemental composition of the powders. The MALDI-MS analysis was performed by employing linear/positive ion modes on a time-of-flight (TOF) mass spectrometer (Microflex, Daltonics Bruker, Bremen, Germany) with a 1.25 m flight tube. Desorption/ionization was achieved by using a 337 nm nitrogen laser with a 3 ns pulsed width. The accelerating potential in the source was maintained at +20 kV. All MALDI-MS spectra were obtained at the average of 200 laser

shots. The laser power was adjusted to slightly above the ionization threshold to obtain good resolution and signal-to-noise (S/N) ratios. The optical densities of the pathogenic bacteria were investigated using an UV-vis (Lambda 20, Perkin Elmer, German). Fourier transform infrared (FTIR) spectra were reported using Spectronic 20 (Perkin Elmer, German). Cells and nanoparticle size and morphology were investigated using a transmission electron microscopy (TEM, Philips CM200/FEG, Netherland).

Bacteria cell culture and cytotoxicity assays

The standard bacteria cultures (*Staphylococcus aureus* (BCRC 10451) and *Pseudomonas aeruginosa* (BCRC 10303)) were purchased from Bioresource Collection and Research Center (BCRC, Hsin-Chu, Taiwan). They were cultivated at 37 °C and maintained on DifcoTM Nutrient broth (Becton and Dickinson, France, 8.0 g per 1.0 L) and Agar plates (Gen Chain Scientific, GCS, New York, USA, with 1.5% agar). The two bacteria were grown individually overnight at 37 °C using agar mediums. The bacteria were dispersed in deionized water (1 mL) using a sterilized needle.

Plate counting method[23]:

The bacteria cells (*S. aureus* and *P. aeruginosa*) were inoculated in deionized and sterile water solutions containing different amounts of $AgFeO_2$ and $AgFeO_2$@PEG (0, 25, 50, 75, and 100 μg mL^{-1}). The mixture was incubated with gentle shaking for 30 min at 37 °C. The number of target organisms present in the sample was determined by the plate counts of *P. aeruginosa* and *S. aureus* with different dilutions on agar (Difco Laboratories). After incubating at 37 °C for 24 h, the presence of the microorganisms was confirmed by the colors of the colonies on the media: *S. aureus* was golden, while *P. aeruginosa* was blue-green on the agar.

Optical density (OD$_{600}$) measurements:

The bacteria cells were inoculated in deionized and sterile water that contained different amounts of AgFeO$_2$ and AgFeO$_2$@PEG (0, 25, 50, 75, and 100 μg mL^{-1}). The mixtures were incubated with gentle before the UV-vis absorption measurements at 600 nm.

Morphological change of pathogenic bacteria by AgFeO$_2$ and AgFeO$_2$@PEG

To visualize the morphology of the tested bacteria in detail after treatment with the synthesized composites, TEM measurements were investigated. In a typical procedure, the bacteria cells (1 mL, 10^4–10^5 cfu mL^{-1}) treated with AgFeO$_2$ and AgFeO$_2$@PEG (0, 25, 50, 75, and 100 μg mL^{-1}) were suspended for 30 min, and then were fixed with 2.5% glutaraldehyde for 30 min. The cells were washed with deionized/sterilized water, then post-fixed with 1% aqueous OsO$_4$ (Fluka) for 30 min and then washed again twice with water. 10 μL of the mixture was placed on the copper grids and then dried for TEM measurements.

Matrix assisted laser desorption/ionization mass spectrometry (MALDI-MS)

Pathogenic bacteria (*S. aureus* and *P. aeruginosa*) were cultivated at 37 °C and maintained on DifcoTM Nutrient broth (Becton, Dickinson, France, 8.0 g per 1.0 L) and Agar plates (Gen Chain Scientific, GCS, New York, USA, with 1.5% agar). The two bacteria were grown individually overnight at 37 °C using agar mediums. The bacteria were dispersed in deionized water (1 mL) using a sterilized needle. The cell numbers (CFU mL^{-1}) were evaluated using plate counting protocol. After 24 h, the cultured bacteria were removed from the agar plate and then dispersed in deionized and sterilized water. The suspension (1 mL) was mixed with AgFeO$_2$ and AgFeO$_2$@PEG (0, 25, 50, 75, and 100 μg mL^{-1}). The solution (10 μL) was well mixed with the matrices (10 μL) and 2 μL of the mixture was loaded onto the MALDI plate, air dried and directly sent for MALDI analysis.

Experimental Section

The antimicrobial effect of $AgFeO_2$ and $AgFeO_2@PEG$ was evaluated by optical density (OD_{600}) and standard micro dilution methods. Equal volumes (1 mL) of each microorganism were colonize to yield a 7×10^6 colony forming unit (CFU) per mL of *P. aeruginosa* or a 6×10^6 colony forming unit (CFU) per mL of *S. aureus*. Then, various concentrations of $AgFeO_2$ and $AgFeO_2@PEG$ (0, 25, 50, 75, and 100 µg mL^{-1}) were mixed and treated in a shaking incubator (24 h, 25 °C, and 150 rpm). Following the treatment, the $AgFeO_2$ and $AgFeO_2@PEG$ were magnetically separated from the mixtures. The solutions were cultivated and the survivals of *P. aeruginosa* or *S. aureus* were measured using UV-vis absorption at 600 nm. After cultivation, the survival of the microorganisms was measured using colony counting and plaque assay methods and expressed as the mean standard deviation.

Results and Discussion

Characterization of AgFeO$_2$ and AgFeO$_2$@PEG NPs

The $AgFeO_2$ and $AgFeO_2@PEG$ NPs were synthesized by one-step hydrothermal method as shown in Scheme 1. The synthesized materials were characterized using the UV-vis absorption, TEM, SEM, EDX and FTIR. $AgFeO_2$ is a semiconductor that belongs to the members of the delafossite family with the expression of ABO_2[24]. Silver cations are alternating layers and edge-sharing FeO_6 octahedra oriented perpendicular to the c-axis. The material could be prepared by hydrothermal method in the presence of NaOH and glycerol. The reason for adding glycerol is to avoid the random aggregation of the prepared nanoparticles. Furthermore, it can work as fuel for the synthesis i.e combustion. Without the addition of polymers, such as polyvinylpyrrolidone (PVP), the preparation of $Ag@Fe_3O_4$, the Ag and the small Fe_3O_4 particles were aggregated in a random way, leading to irregular shapes and aggregation of products.
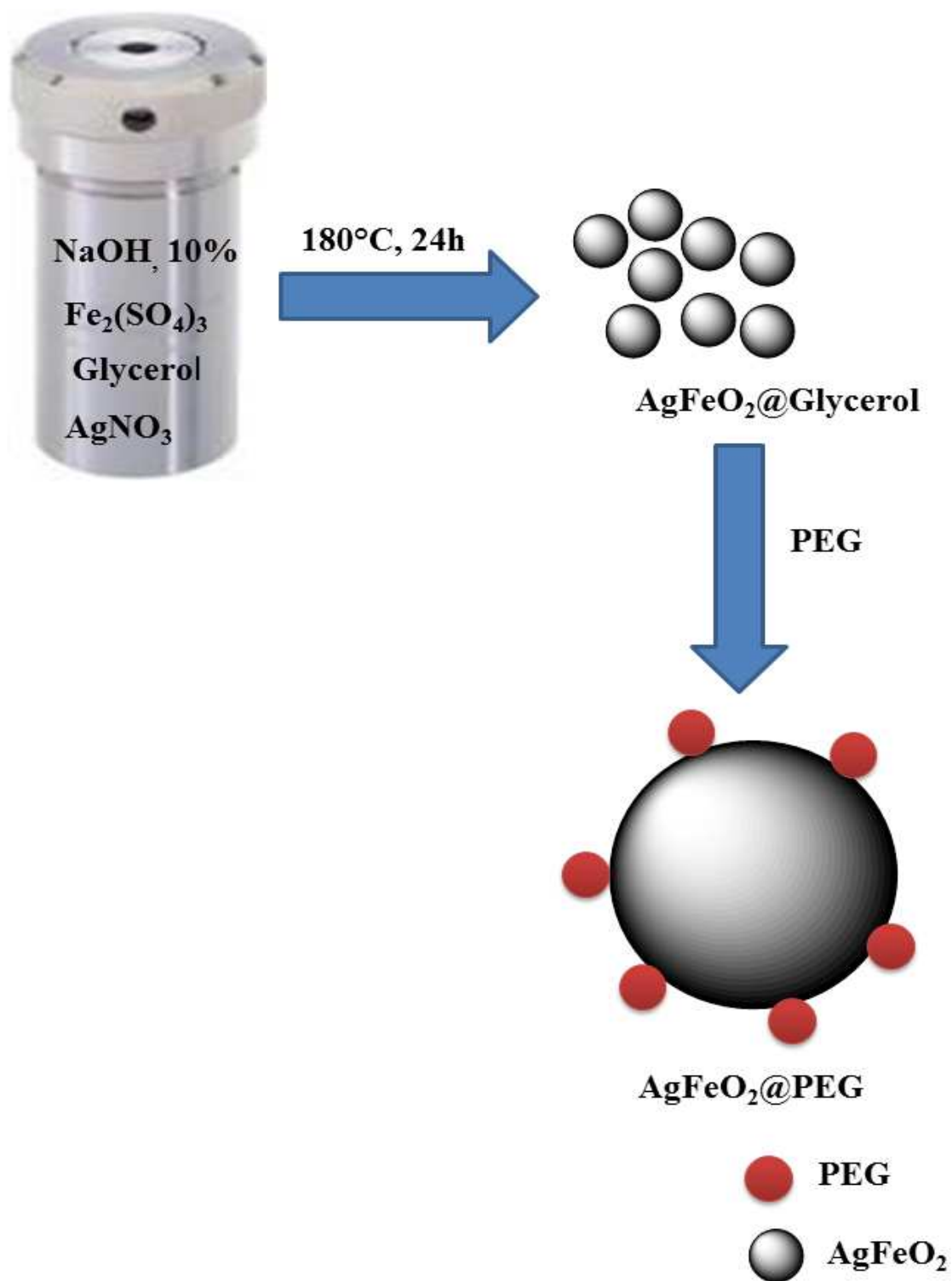
Scheme 1. Schematic representation of hydrothermal synthesis of AgFeO$_2$@PEG

The mechanistic study of $AgFeO_2$ preparation is unknown so far. TEM monograph (Fig.1A) shows that the diameter of the $AgFeO_2$ nanoparticles is around 50–100 nm with average size about 26 nm as shown in Fig.S1. The monograph of the $AgFeO_2$ was characterized by SEM (Fig.1B). The chemical composition of $AgFeO_2$ was investigated by EDX analysis (Fig.S2). The elemental analysis displays the composition is Ag, Fe and O. As shown in Fig. S2, the characteristic signals for Ag, oxygen and Fe are clearly detected at 3, 0.5 KeV and 0.8 for Fe La, 6.5 Fe K_a and 7.0 Fe K_b, respectively. The UV-vis absorption spectrum of the $AgFeO_2$ nanoparticles (Fig. 1C) shows a broad absorption band (300-700 nm). The broad absorption may be due to the presence of particles with different sizes [24]. The spectrum shows maximum absorption at 350 nm. It is important to mention the types of forces that govern the PEG-$AgFeO_2$ interactions. In general, biomolecules natively possess specific interactions with metals and thus can be high enough for interactions. These forces enhanced for NPs that has large surface area. These forces reinforce each other. The interaction of Ag NPs and biolmoecules such as peptide or cellulose were reported. The interactions are high mainly due to the negative charges of the biomolecules and the positive charge or the surface plasmonic resonance (SPR) of Ag NPs [25].
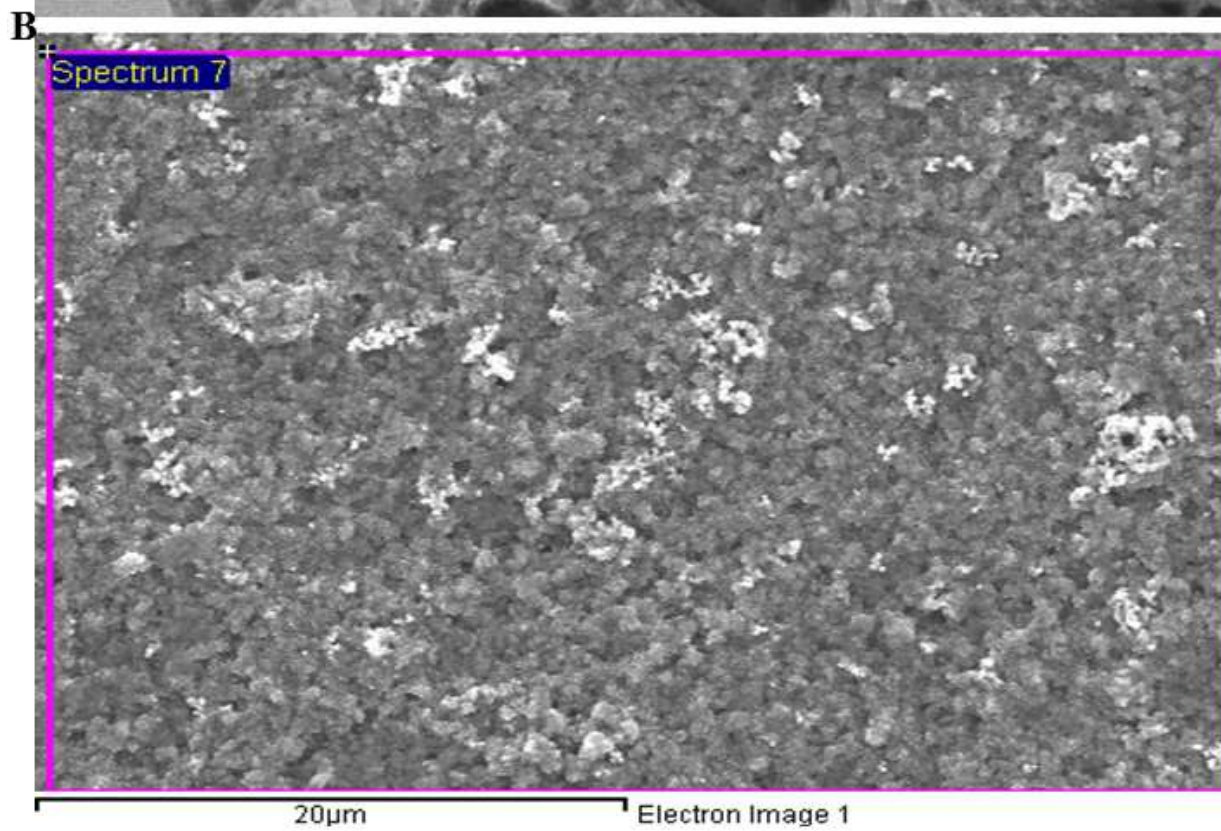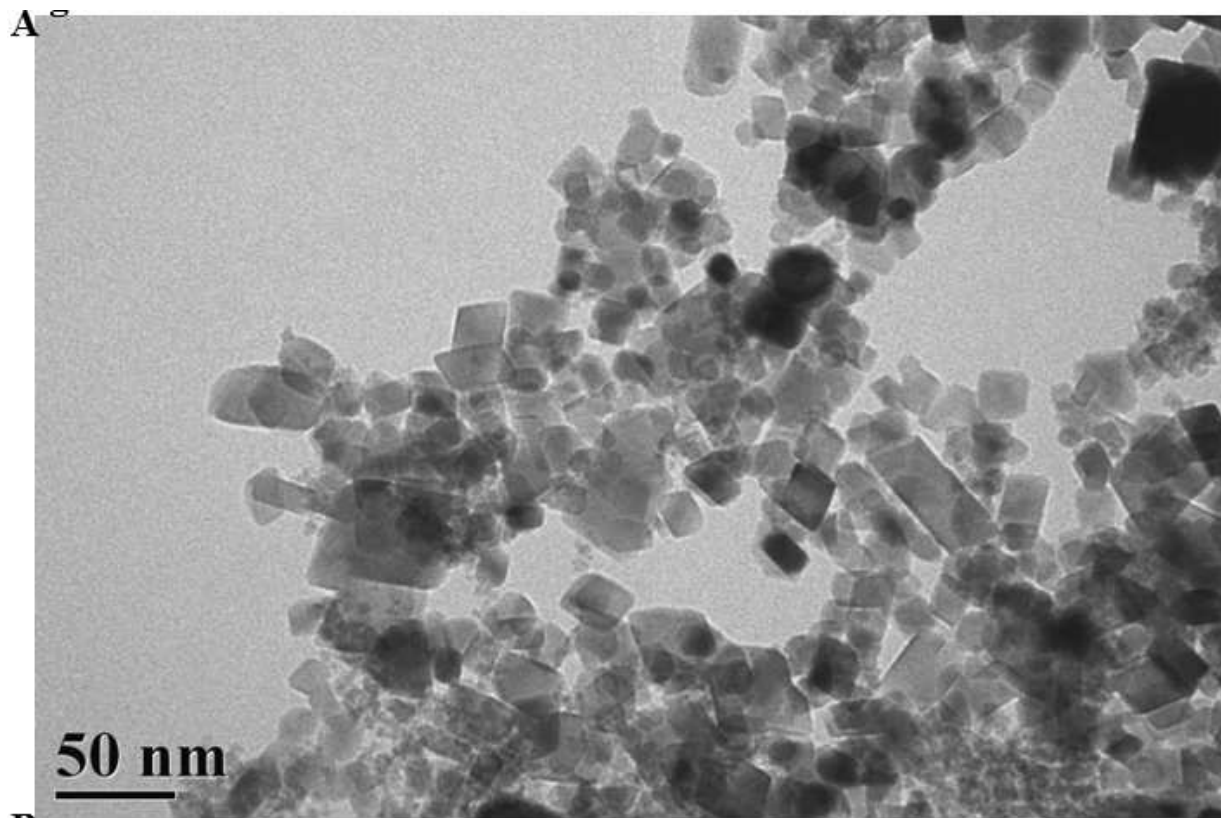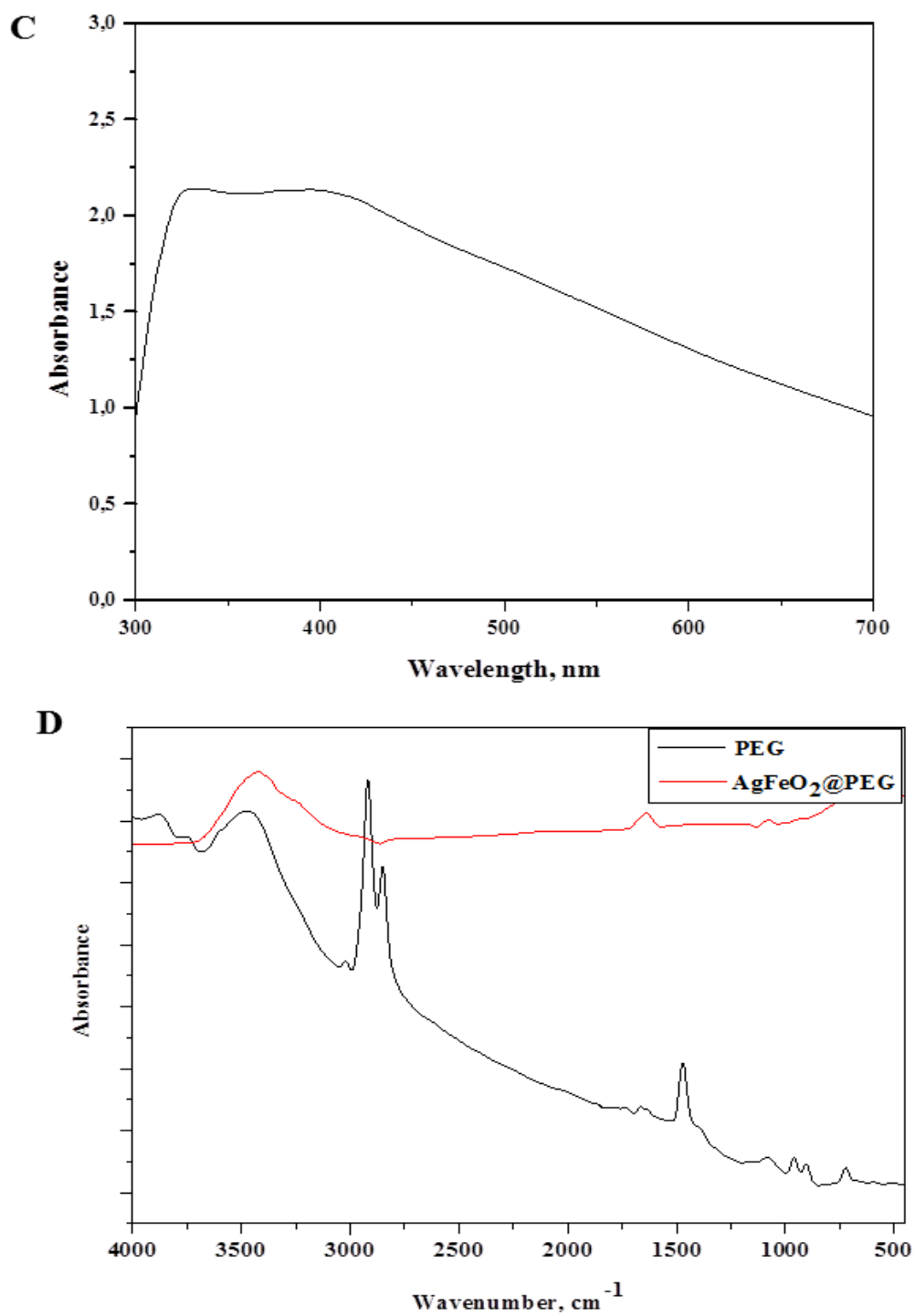
Fig.1. Characterization of AgFeO$_2$ using (A) TEM, (B) SEM, (C) UV-vis absorption and (D)

FTIR spectroscopy .

Recently, Shi et.al used $AgFeO_2$ as substrates for surface enhanced Raman spectroscopy (SERS) as it absorbs laser with wavelength 633 nm[24]. Because of its uncharged hydrophilic residues, high surface mobility and biocompatibility, polyethylene glycol (PEG) has been widely used to improve the water dispersity and steric stability of magnetic NPs or noble metal NPs [26]. The surface modification of $AgFeO_2$ with PEG was confirmed in Fig.1D; it shows the FTIR spectra of PEG-20000 and the typical $AgFeO_2$@PEG hybrid NPs. The prominent peak that appeared in the hybrid NPs at 581 cm^{-1} is from the iron oxide skeleton (–O–Fe), indicating the existence of $AgFeO_2$ nanocrystals. The bands around 1347 cm^{-1} and 1112 cm^{-1} originated from the asymmetric and symmetric stretching of the –C–O–C– repeating units on the PEG chains present in the hybrid NPs. The strong and broad band centered around 1651 cm^{-1} was assigned as the conjugated carbon in the shell of NPs. The broad band around 3450 cm^{-1} was from the hydroxyl groups at the end of PEG chains and from the carboxyl groups. Recently (2014), Sun el.al reported the decoration of Ag NPs with homopolymer vesicles called poly(2-(2-ethoxyethoxy)ethyl acrylate) (PEEA) in water/tetrahydrofuran (THF) solvent mixture via self-assembly procedure. They found that the –COOH end groups on the surface of the homopolymer vesicle facilitate the growth of ultrafine silver nanoparticles because of the electrostatic interactions between the negatively charged carboxyl group and positively charged Ag^+ ions [27]. Roy and Banerjee reported that silver ions are complexed with the carboxylate group of the Fmoc-Phe-OH gelator [28]. The strong interactions reveal slow decomposition [29].

Antimicrobial evaluation of $AgFeO_2$ and $AgFeO_2$@PEG by optical density (OD_{600}) and plate counting

In order to probe the antibacterial activity of $AgFeO_2$ and $AgFeO_2$@PEG, optical density (Fig.2A) and plate counting method (Fig.2B) were used. The OD_{600} is measured in a spectrophotometer at 600 nm. Optical density (OD_{600}, Fig.2A) is based on measuring the turbidimetry. The underlying principle is that most of the light scattered by the cells. The OD_{600} of a bacterial culture is thus primarily not an absorbance, as in the case of a dissolved chromophore. It is therefore not correct (even though unfortunately common) to designate the OD_{600} of a culture an absorption; the most appropriate term would indeed to be turbidity. OD_{600} of *P. aeruginosa* (Fig.2A(a)) and *S. aureus* (Fig.2A(b)) for $AgFeO_2$ show increase in the value of optical density. The increment is due to disruption of the cells content, thus OD_{600} is increased.
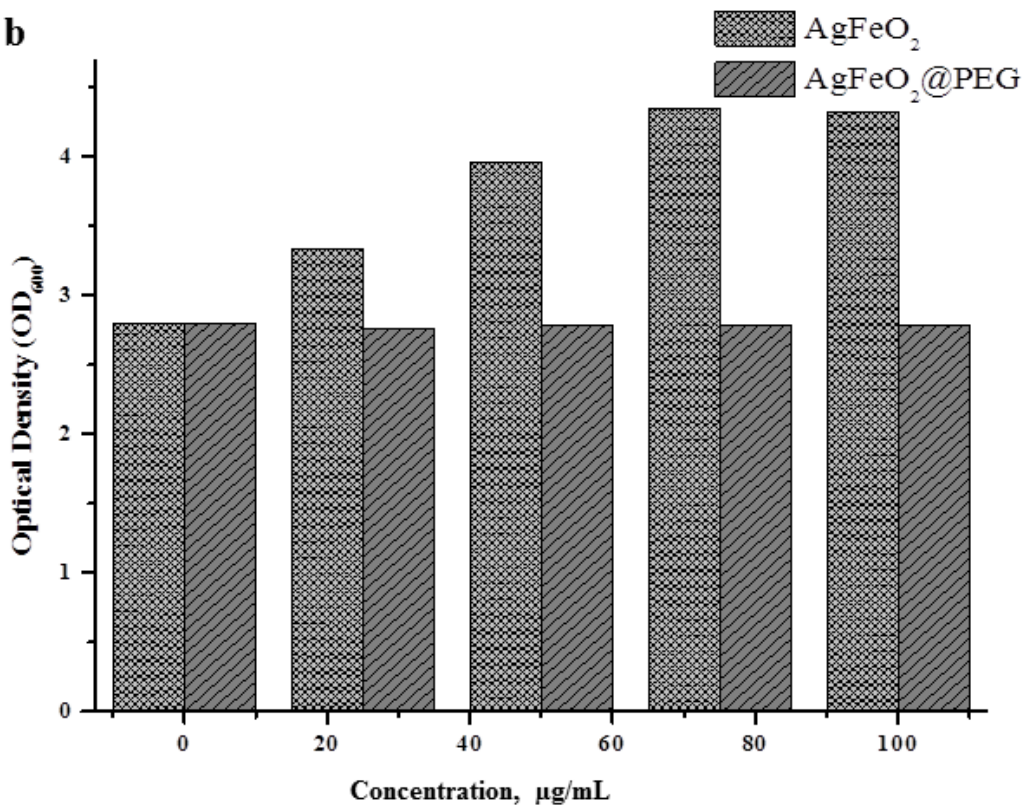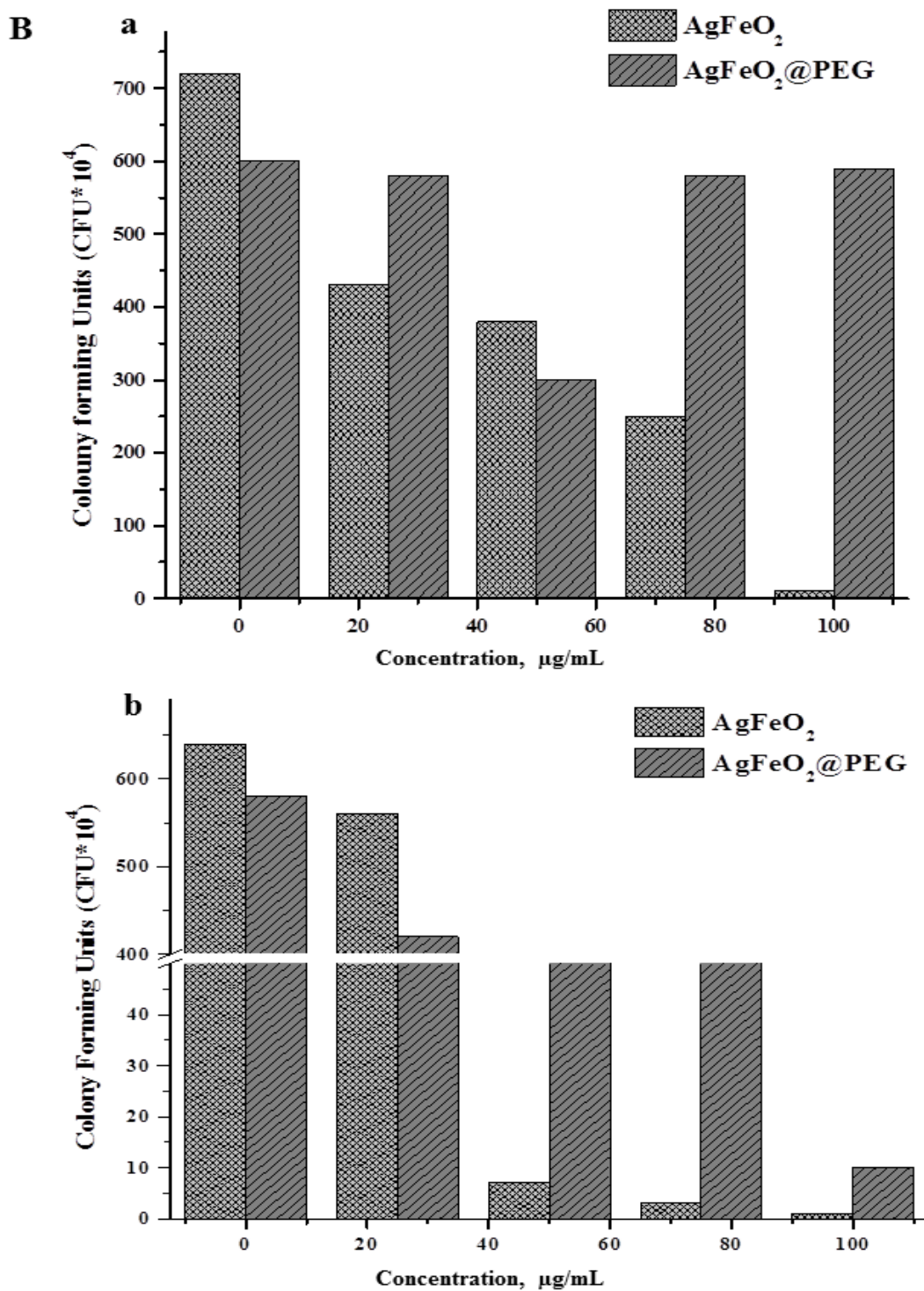
Fig.2

A
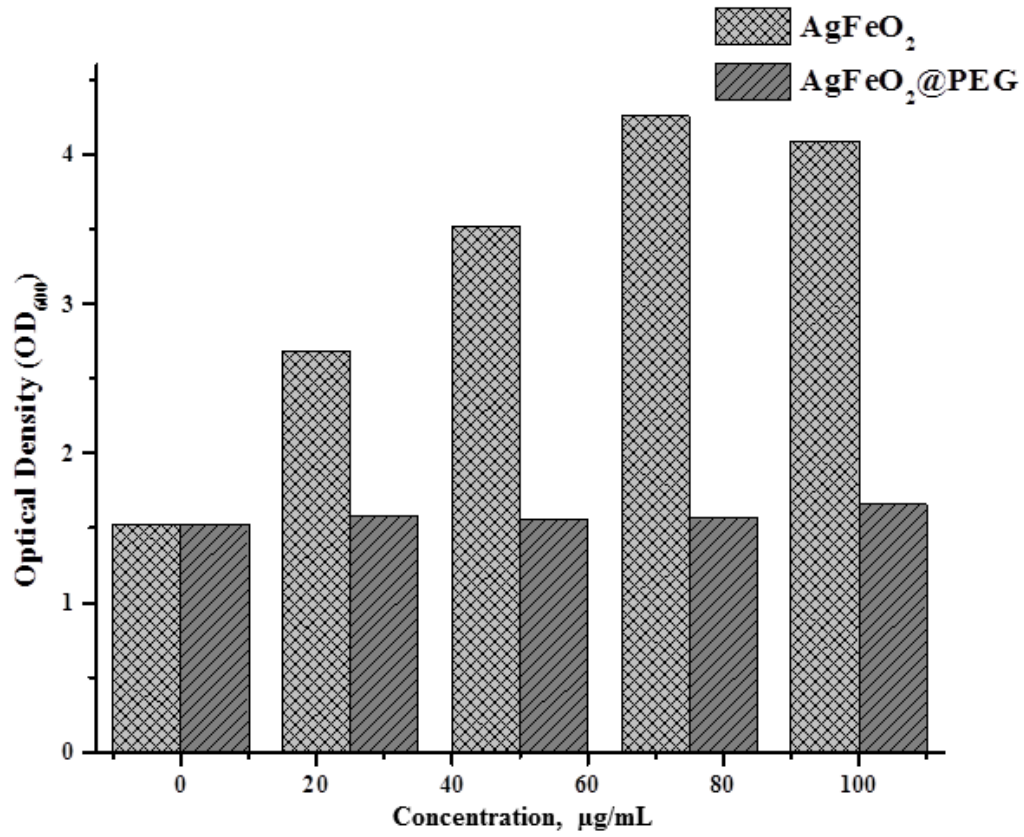
Fig.2. Cytotoxicity assay using (A) Optical density (OD$_{600}$) and (B) plate counting protocol, for (a) *P. aeruginosa* and (b) *S. aureus.* .

In contrast, AgFeO$_2$@PEG shows no effect on OD$_{600}$ of both strains i.e *P. aeruginosa* (Fig.2A(a)) and *S. aureus* (Fig.2A(b)). The increment of OD$_{600}$ is a function on the concentration of AgFeO$_2$. The data show that minimum inhibition concentrations (MIC) of both strains are 25 µg/mL. The reason for the passive effect of AgFeO$_2$@PEG may be due to the Ag substrate on the PEG matrix or may be due to the well dispersion of AgFeO$_2$@PEG than AgFeO$_2$. Thus, we confirmed the result by plate counting approach. However, plate counting is time consuming (24h), but it is more accurate than turbidimetry. The cytotoxicity of AgFeO$_2$ and AgFeO$_2$@PEG against *P. aeruginosa* (Fig.2A(a)) and *S. aureus* (Fig.2A(b)) were investigated. The plate counting for *P. aeruginosa* (Fig.2A(a)) shows a dramatic decrease with the increment on the AgFeO$_2$ concentration (0, 25, 50, 75, 100 µg/mL). The data confirm that MIC is 25 µg/mL. The data in Fig.2A(a) also confirmed the biocompatibility of AgFeO$_2$@PEG against *P. aeruginosa*. The toxicity of AgFeO$_2$ against *S. aureus* is well confirmed by plate counting as shown in Fig.2A(b). In a stark contrast, AgFeO$_2$@PEG display nanocytotoxicity against *S. aureus* as shown in Fig.2A(b). This contradict may be due to the sensitivity of the two techniques or the intrinsic behavior of *S. aureus* over than *P. aeruginosa*. Thus, we investigate the morphology changes by TEM analysis.
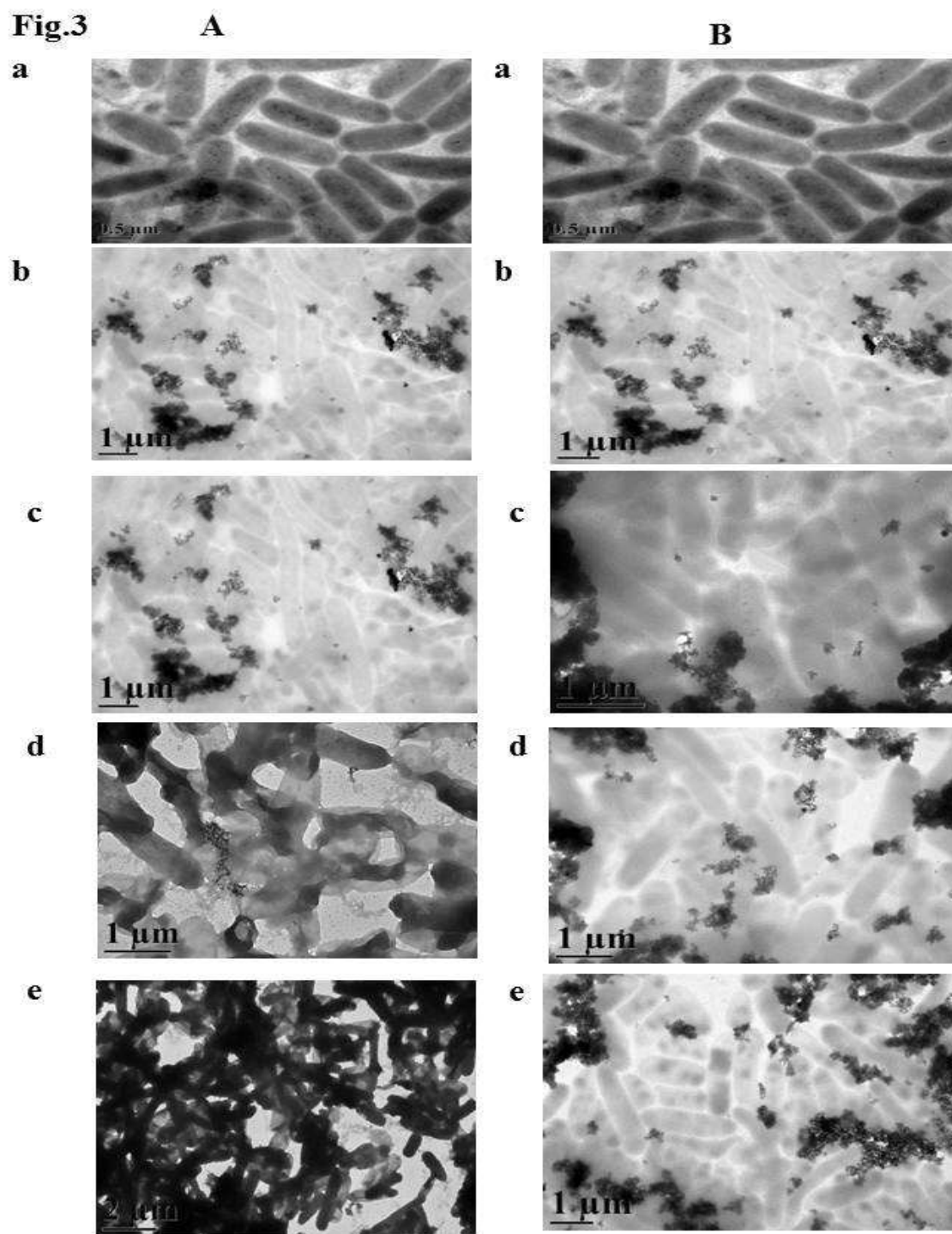
Fig.3   A   B

Fig.3. Morphology changes of *P. aeruginosa* upon addition of (A) AgFeO$_2$ and (B) AgFeO$_2$@PEG with different concentration (a) 0, (b) 25, (c) 50, (d) 75, and (e) 100 µg/mL.
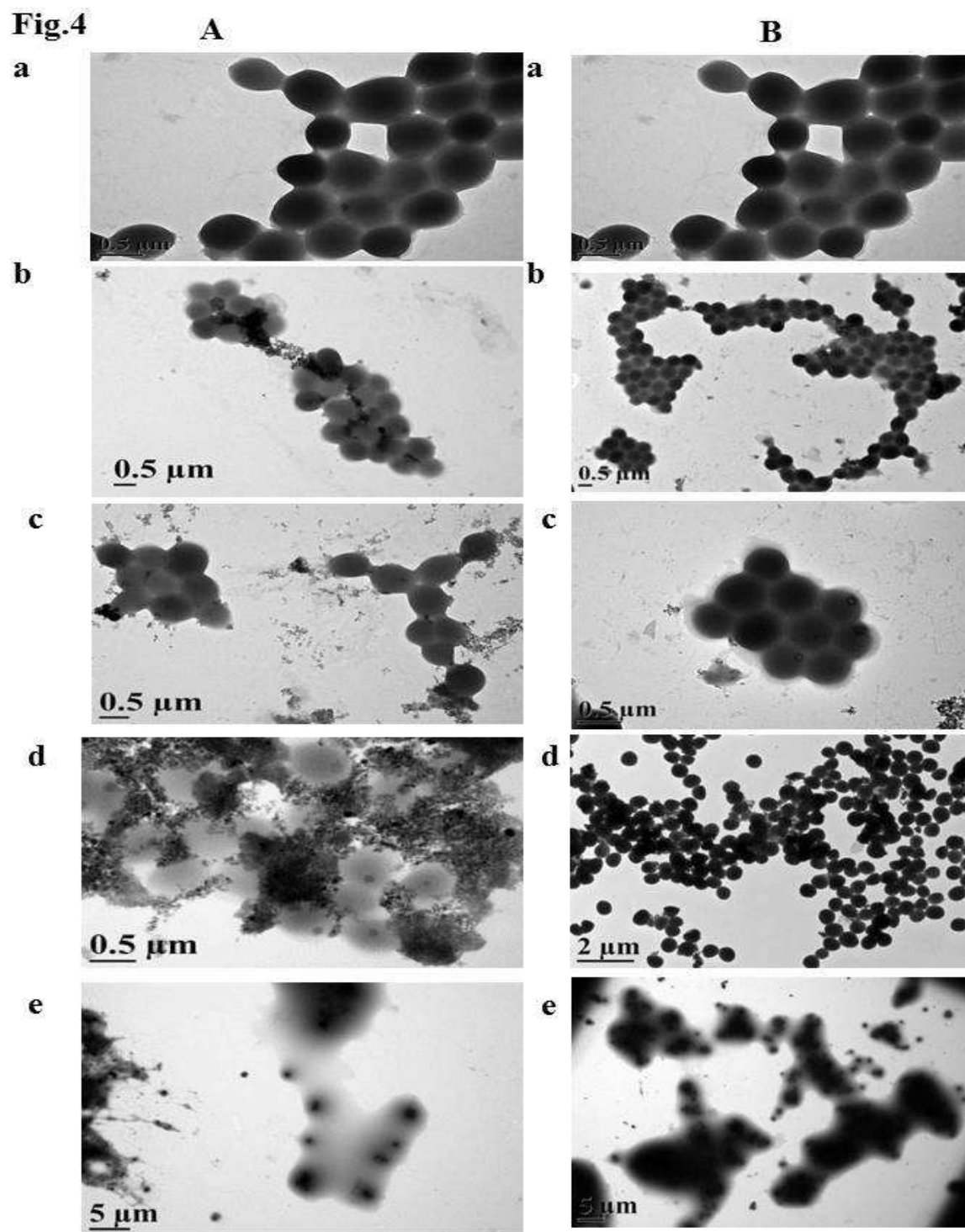
Fig.4. Morphology changes of *S. aureus* upon addition of (A) AgFeO$_2$ and (B) AgFeO$_2$@PEG

with different concentration (a) 0, (b) 25, (c) 50, (d) 75, and (e) 100 µg/mL.

Antimicrobial mechanism of AgFeO$_2$ and AgFeO$_2$@PEG by TEM

The changes of the cell morphology were explored by TEM. The morphological change of *P. aeruginosa* (Fig.3) and *S. aureus* (Fig.4) was monitored as a function of concentration (0, 25, 50, 75, 100 µg/mL). The TEM images of *P. aeruginosa* show complete rupture of the cells structure using bare AgFeO$_2$ at high concentration (75 and 100 µg/mL). The cell membrane was seriously damaged and the bacteria shapes were irregular. This observation is already confirmed from UV-vis absorption and plate counting. In the other side, the cells morphology shows no change in the case of AgFeO$_2$@PEG that confirms the biosafety of these nanoparticles. The majority of the bare *S. aureus* preserves their rod-shaped morphology at low concentration, while their structures are completely ruptured at high concentration (Fig.4). The bacteria body is fractured leading to the leakage of interior components. Park et.al reported the morphology changes of *E. coli* with Ag NP@MHC [9]. They claimed that *E. coli* cannot uptake Ag NP@MHC due to its large size and that the primary means of inactivation by Ag NP@MHC is through interaction with the outer membrane of *E. coli*. It is a general observation that in the absence of surface coating, AgFeO$_2$ NPs have the tendency to agglomerate due to their large surface area to volume ratios. The PEG polymer coating can prevent the agglomeration and provides stability to ferrite nanoparticles. Li et.al [30] reported that Ag$^+$ are easily accumulated around the living bacterial cells due to the bacteria surface's negative charges, which were originated from the carboxyl and phosphoric acid groups in the outer membrane. The adsorbed Ag$^+$ can interact with the thiol (–SH) group of the cysteine chain by replacing the hydrogen atom to form –S–Ag, thus hindering the enzymatic function of the affected protein to inhibit growth of the bacteria cells[30].
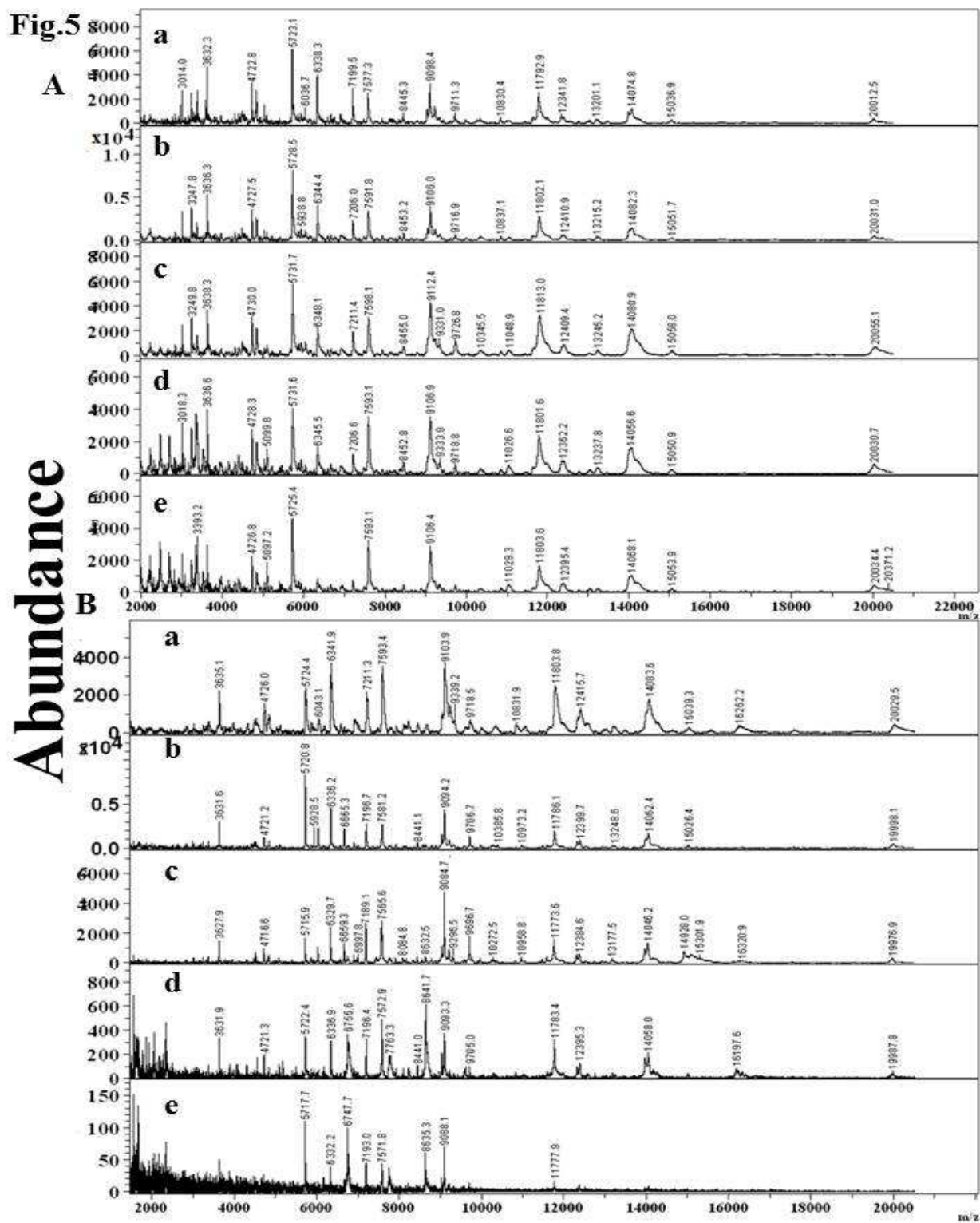
Fig.5. MALDI-MS profile of *P. aeruginosa* upon addition of (A) AgFeO$_2$ and (B) AgFeO$_2$@PEG upon different amount (a) 0, (b) 25, (c) 50, (d) 75 and (e) 100 µg/mL.

Proteomics analysis of pathogenic bacteria

MALDI-MS analysis of pathogenic bacteria is simple, rapid, sensitive and can provide information for the bacteria contents[31]. The importance of this technique is not to record the cytotoxicity, but to probe the interactions between the cells proteins and the nanoparticles via proteomic analysis. When the cells were mixed with matrix acid, it causes hydrolysis. Then, the lysate interact with the nanoparticle surface i.e protein corona. The protein profile of *P. aeruginosa* (Fig.5) and *S. aureus* (Fig.S3) were recorded. The profile of *P. aeruginosa* (Fig.5) upon addition different concentration of bare $AgFeO_2$ reveals the cell contents are the same but increases in the small protein or peptide in the mass range 2000-4000 *m/z*. This observation clarified the reason for the optical density increment (Fig.2A), i.e cell rupture. The situation of $AgFeO_2$@PEG is different. The profile at high concentration shows suppression of the peaks. The reason may be due to the presence of PEG to suppress the ionization of the cell lysate. The protein corona of *S. aureus* with $AgFeO_2$ show that the cell contents are the same but with increase of small protein peaks to reveal cell rupture. MALDI-MS clearly indicate the formation of the protein corona on the surface of $AgFeO_2$. The surface coating of $AgFeO_2$ NPs with a PEG biopolymer shell is an effective way to improve their biocompatibility and water dispersity[32].

Mechanistic study

McShan et.al summarized the mechanism of Ag NPs cytotoxicity. The nanotoxicity is due to many reasons such as the oxidation of their surface by O_2 and other molecules in the environmental and biological systems leading to the release of Ag^+. Thus, it is the most reasonable mechanism for $AgFeO_2$ NPs. They observed also other mechanisms such as oxidative stress through the generation of reactive oxygen species and causes damage to cellular components including DNA damage, activation of antioxidant enzymes, depletion of antioxidant

molecules (e.g., glutathione), binding and disabling of proteins, and damage to the cell membrane [33]. In order to address a reasonable mechanism, we attempted to probe the cytotoxicity of $AgFeO_2$ using the different analytical tools. It is well known that the Ag-based nanomaterials possess strong inhibitory and antimicrobial effects because the binding of Ag NPs to bacterial DNA that may not only inhibit some important transport processes including phosphate and succinate uptake, but also can interact with cellular oxidation processes as well as the respiratory chains. The bacterial survival can be monitored by the optical density at 600 nm (OD_{600}). The data reveals that the higher concentration of the hybrid NPs, the more effective the inhibition of the bacterial growth because of more cells ruptures. It is also reported that Ag cytotoxicity is due to the interaction with the cell membrane. Silver nanoparticle-decorated magnetic-silica Janus nanorods (AgNPs@Fe_3O_4–SiO_2 JNRs) showed a strong affinity binding to bacteria, and highly effective and long-term antimicrobial activity against bacteria [12]. Prucek et.al reported the antibacterial activity of binary nanocomposite of the Ag@Fe_3O_4 and γ-Fe_2O_3@Ag type employing polyacrylate acid as an effective linker[34]. They found that both synthesized nanocomposites exhibited the highest antibacterial and antifungal activities among all magnetic silver nanocomposites developed so far. They reported that MIC for those materials against broad number of bacteria cells was 15-125 mg/L. Moreover, we reported a lower MIC than some of those values i.e 20 mg/L [34]. The major challenge to draw a precise conclusion of the NPs cytotoxicity is due to many reasons. The toxicity is dependent on concentrations and size of the prepared materials. It is also dependent on the bacterial cell types, analytical tools that were used for the assessments. The antibacterial activity can be also due to presence of other additives such as light-activated antimicrobial materials such as porphyrin [35]. Agnihotri et.al reported that not only size but also the strain effect the NPs cytotoxicity [36].

Advantages of AgFeO$_2$

However, there are many methodologies for water treatment, but inorganic nanoparticles are promising. For instance, UV treatment alone can push bacteria into a dormant state instead of killing them, and that in some cases; the bacteria can later revive and proliferate [37]. Thus, chemical treatment is promising as it kills the pathogenic cell by destroying the bacterial cell membrane. The AgFeO$_2$ nanoparticles offer many merits than either Ag NPs or Fe$_3$O$_4$ NPs which are summarized as below: (1) Comparing Ag NPs with AgFeO$_2$, the aggregation of the nanoparticles during application is minimized. (2) Separation and recovery of AgFeO$_2$ is easier to operate after using in water disinfection than that of Ag NPs. Therefore, the AgFeO$_2$ is an excellent bactericidal material with powerful antibacterial ability, magnetic response and stability. These features could also minimize the Ag pollution to the environments too. (3) It offers remarkable antibacterial properties. As a comparison, the MIC is approximately 800 μg ml^{-1} for commercially available antibacterial particles [38] and bare Fe$_3$O$_4$ nanoparticles did not show any biocidal activity up to 1000 μg ml^{-1} i.e highly biocompatibility [39-40]. (4) The nanotoxicity can also mitigate by functionalization with PEG. (5) The AgFeO$_2$ can be functionalized with a wide range of different biomolecules to increase their applications including water purification systems, surgery instruments, wound dressings and medical devices such as oral and bone implant materials. (8) it circumvent the drawbacks of Ag nanoparticles such as (a) their toxic effects on human cells by functionalization and (b) their low yield for penetration through the bacterial biofilms that can be improved by targeting the material using external magnetic field. (9) Although Fe$_3$O$_4$ is non-toxic and easily prepared, but they are easily

oxidized due to the presence of Fe^{2+}. While the iron species exist in $AgFeO_2$ is Fe^{3+}, thus toxicity of $AgFeO_2$ is mainly due to Ag. This species can be coordinated with PEG that mitigates the antibacterial of the $AgFeO_2$ nanocomposites.

Conclusion

We successfully synthesized $AgFeO_2$ nanoparticles and modified their surface with polyethylene glycol (PEG). The antibacterial assessments showed highly potential of the synthesized materials. This character can be tuned by functionalization with PEG biomolecules. $AgFeO_2$ offers high biocidal over than Ag nanoparticles or commercial antibacterial. Combining the high antibacterial and magnetic properties, the $AgFeO_2$ offers easier separation and high efficiency. It shows wide spectrum potency and high stability.

Acknowledgments

References

1. (a) K. J. Simmons, I. Chopra, C. W. G. Fishwick,. Nature Review, 2010, **8**, 501-510; (b) Editorial, Bacteria not welcome at the MRC?, Nature Reviews Microbiology 4, 2006, doi:10.1038/nrmicro1332

2. A. K. Singh, P. Singh, S. Mishra and V. K. Shahi. *J. Mater. Chem.*, 2012, **22**, 1834–1844

3. R. B. Wang, L. Wang, L. Z. Zhou, Y. Su, F. Qiu, D. L. Wang, J. L. Wu, X. Y. Zhu and D. Y. Yan. *J. Mater. Chem.*, 2012, **22**, 15227–15234

4. (a) P. Kaali, E. Stromberg, R. E. Aune, G. Czel, D. Momcilovic and S. Karlsson, Polym. Degrad. Stab. 2010, **95**, 1456– 1465; (b) H. J. Jeon, S. C. Yi and S. G. Oh. Biomaterials, 2003, **24**, 4921– 4928; (c) M. S. Lee, S. S. Hong and M. Mohseni. J. Mol. Catal. A: Chem., 2005, **242**, 135–140.

5. (a) M. Niu, X. G. Liu, J. M. Dai, H. S. Jia, L. Q. Wei and B. S. Xu. Carbohydr. Polym., 2009, **78**, 54–59; (b) T. Yuranova, A. G. Rincon, C. Pulgarin, D. Laub, N. Xantopoulos, H. J. Mathieu and J. Kiwi. J. Photochem. Photobiol., A, 2006, **181**, 363–369.

6. M. AbuEl-Hassan, M. B. Mohamed, M. Fawzy, D. Abdelrehim and M. Abdel-Mottaleb. RSC Adv.**, 2015,** DOI**:** 10.1039/C4RA13117G; (b) A. Hameau, V.Collière, J. Grimoud, P. Fau, C. Roques, A.-M. Caminade and C.-O. Turrin , RSC Adv., 2013,**3**, 19015-19026 *; (c)* A. Rajendran and D. K. Pattanayak, RSC Adv., 2014,**4**, 61444-61455; (e) R. Xiong, C. Lu, Y. Wang, Z. Zhou and X. Zhang, J. Mater. Chem. A, 2013, **1**, 14910–14918; (f) P. Jain and T. Pradeep, Biotechnology and Bioengineering , 2005, **90** , 59-63 , 2010.; (g) H. Luo, C. Gu, W. Zheng, F. Dai, X. Wang and Z. Zheng, RSC Adv., 2015,**5**, 13470-13477 ; (h) J. Yang, H. Zheng, S. Han, Z. Jiang and X. Chen, RSC Adv., 2015,**5**, 2378-2382*;* (i) G. M. Raghavendra, T. Jayaramudu, K. Varaprasad, G.S. M. Reddy and K. M. Raju, RSC Adv., 2015,**5,** 14351-14358*;* (j) S. Barua, P. Chattopadhyay, M. M. Phukan, B. K. Konwar, J. Islam and N. Karak, RSC Adv., 2014,**4**, 47797-47805; (k) M. M. Najafpour, A. Zahraee, E. Amini, M. M. Ahari-Mostafavi and M. Kompany-Zareh, RSC Adv.**,** 2014,**4**, 64688-64691; (l) L. He, L. F. Dumée, D. Liu, L. Velleman, F. She, C. Banos, J. B. Davies and L. Kong . RSC Adv., 2015,**5**, 10707-10715

7. R.Xiong, Y. Wang, X. Zhang, C. Lu, RSC Adv.,2014,**4**,22632–22641

8. M. L. Chen, M. D. Dong, R. Havelund, V. R. Regina, R. L. Meyer, F. Besenbacher and P. Kingshottt. Chem. Mater. 2010, **22**, 4214–4221

9. H. H. Park, S.J. Park, G.P.Ko, K. Woo. *J. Mater. Chem. B*, 2013, **1**, 2701–2709

10. M. Kooti, P. Kharazi , H. Motamedi. *J. Twain. Inst. Chem. Eng.* 2014, http://dx.doi.org/10.1016/j.jtice.2014.04.006

11. W. Fang, J. Zheng, C. Chen, H. Zhang , Y. Lu , L. Ma, G. Chen. J. Magnetism. Magnetic. Mater. 2014, **357**,1–6

12. M. Kooti, P. Kharazi, H. Motamedi. *J. Mater. Sci. Technol.,* 2014, http://dx.doi.org/10.1016/j.jmst.2013.12.007

13. H. Wang, J. Shen, G.Cao, Z. Gai, K. Hong, P. R. Debata, P. Banerjee, S. Zhou, J. Mater. Chem. B, 2013, **1**, 6225–6234

14. X. Wang, Y. Dai, J. Zou, L. Meng, S. Ishikawa, S. Li, M. Abuobeidah, H. Fu. RSC Adv., 2013, **3**, 11751–11758

15. L. Lin, H. Cui, G. Zeng, M. Chen, H. Zhang, M. Xu, X.Shen, C. Bortolini, M. Dong. J. Mater. Chem. B, 2013, **1**, 2719–2723

16. L. Zhang, Q. Luo, F. Zhang, D.M. Zhang, Y.-S. Wang, Y.-L. Sun, W.-F. Dong, J.-Q. Liu, Qi-Sheng Huo, Hong-Bo Sun. *J. Mater. Chem*., 2012, **22**, 23741–23744

17. M. N. Nadagouda, C. Bennett-Stamper, C. White, D, Lytle. *RSC Advances*, 2012, **2**, 4198–4204

18. S. Senapati, S. K. Srivastava, S. B. Singh, H. N. Mishra. *J. Mater. Chem*., 2012, **22**, 6899–6906

19. L. Wang, J. Luo, S. Shan, E. Crew, J. Yin, C. J. Zhong, B. Wallek, S. S.S. Wong. Anal. Chem. 2011, **83**, 8688–8695

20. H. Xia, B. Cui, J. Zhou, L. Zhang, J. Zhang, X.Guo, H. Guo,. Applied Surface Science 2011, **257**, 9397– 9402

21. Y. Liu, Z. Ren, Y. Wei, B. Jiang, S. Feng, L. Zhang, W. Zhang, H. Fu. J. Mater. Chem., 2010, 20, 4802–4808

22. A. Alonso, X. Muñoz-Berbel, N.Vigués, R. Rodríguez-Rodríguez, J. Macanás, M. Muñoz, J. Mas, D. N. Muraviev. *Adv. Funct. Mater.* 2013, **23**, 2450–2458

23. H. N. Abdelhamid, H.F. Wu. Colloids and Surfaces B: Biointerfaces, 2014, **115**, 51–60

24. Z. Shi, T. Wang, H.Lin, X. Wang, J. Ding, M. Shao. Nanoscale, 2013, **5**, 10029–10033

25. (a) T.Y. Shih and S.L. Tsai, <u>RSC Adv.</u>, 2014, **4**, 40994-40998; (b) B. Adhikari and A. Banerjee, Chem. Eur. J., 2010, **16**, 13698 – 13705; **(c)** H.N. Abdelhamid, H.F. Wu, Materials Science and Engineering: C 2014, 45, 438-445

26. J. J. Khandare, A. Jalota-Badhwar, S. D. Satavalekar, S. G. Bhansali, N. D. Aher, F. Kharas and S. S. Banerjee. Nanoscale, 2012, **4**, 837 -844.

27. H. Sun, L. Fan, K. Zou, H. Zhu and J. Du, Decoration of homopolymer vesicles by antibacterial ultrafine silver nanoparticles, <u>RSC Adv.</u>**,** 2014, **4**, 41331-41335

28. S. Roy and A. Banerjee, Soft Matter, 2011, **7**, 5300–5308

29. T. U. B. Rao, B. Nataraju, and T. Pradeep, J. AM. CHEM. SOC. 2010, **132**, 16304–16307

30. W. R. Li, X. B. Xie, Q. S. Shi, H. Y. Zeng, Y. S. Ou-Yang and Y. B. Chen. Appl. Microbiol. Biotechnol., 2010, **85**, 1115-1122.

31. (a) H.N. Abdelhamid, M.S. Khan, H.F. Wu, RSC advances 2014, **4**, 50035-50046; (b) H.N. Abdelhamid, H.F. Wu, TrAC Trends in Analytical Chemistry 2015, **65**, 30-46; (c)

H.N. Abdelhamid, H.F. Wu, Analyst, 2015, **140**, 1555-1565; (d) B.S. Wu, H. N. Abdelhamid, H.F. Wu. RSC advances, 2014, **4**, 3722-3731

32. V. M. Ragaseema, S. Unnikrishnan, V. K. Krishnan andL. K. Krishnan. Biomaterials, 2012, **33**, 3083-3092.

33. D. McShan, P. C. Ray, H. Yu, Journal of Food and Drug Analysis, 2014, **22**, 116–127

34. R. Prucek, J. Tuček , M. Kilianová, A. Panáček , L. Kvítek , J. Filip , M. Kolář , K. Tománková , R. Zbořil. Biomaterials. 2011, **32**, 4704-4713

35. O. Lyutakov, O. Hejna, A. Solovyev, Y. Kalachyova and V. Svorcik. RSC Adv., 2014,4, 50624-50630

36. S. Agnihotri, S. Mukherji and S. Mukherji. RSC Adv., 2014, **4**, 3974-3983

37. S. Zhang , C. Ye , H. Lin , L. Lv , and X. Yu, Environ. Sci. Technol., 2015, **49**, 1721– 1728

38. M. Kawashita, S. Toda, H.M. Kim, T. Kokubo, N. Masuda. *J. Biomed. Mater. Res.* A, 2003, **66,** 266–74

39. J. Gopal, H. N. Abdelhamid, P. Y. Hua, H.F. Wu. *J. Mater. Chem. B*, 2013, **1**, 2463-2475

40. M. L. Bhaisare, H. N. Abdelhamid, B.S. Wu, H.F. Wu. *J. Mater. Chem. B*, 2014, **2**, 4671-4683.